

Microfluidic light scattering as a tool to study the structure of aqueous polymer solutions [☆]

Alexander I. Norman ^{*,1}, Wenhua Zhang, Kathryn L. Beers, Eric J. Amis ^{*}

Polymers Division, National Institute of Standards and Technology, 100 Bureau Drive, Gaithersburg, MD 20899-8542, USA

Received 14 November 2005; accepted 14 February 2006

Available online 10 March 2006

Abstract

A small-angle light scattering (SALS) apparatus, coupled with a specially designed microfluidic device is shown to monitor the formation and subsequent size distribution of giant multilamellar vesicles of a diblock copolymer in aqueous solution. The closed-face design, fabricated between glass slides using a UV-curable optical adhesive, incorporates multiple inlets, a mixing system, and a viewing window to perform on-line SALS. The mixing of each component is tested using polystyrene latex microspheres. Vesicles of the block copolymer, EO₆BO₁₁ in aqueous solution are formed on the SALS chip and the pair distance distribution function determined using an inverse Fourier transformation of the scattered intensity to quantify the population and distribution for a range of vesicle sizes. These experiments provide demonstrations of how SALS on a microfluidic device can be used as a rapid screening tool to optimize processing conditions for a range of polymer solutions.

© 2006 Elsevier Inc. All rights reserved.

Keywords: Microfluidics; Small-angle light scattering; Vesicles; Screening tools

1. Introduction

Microfluidic technologies based on devices transporting fluids through micrometer sized channels are rapidly evolving and are used widely in biology [1] and biotechnology due to their ability to handle small quantities [2]. Examples of applications include cell sorting [3], high-throughput screening [4], and chemical reactions [5]. There remain many opportunities to exploit microfluidics for applications in polymer science.

Traditional methods used for the fabrication of microfluidic devices involve silicon and glass etching techniques [6,7]. Such processes are costly, labor intensive and require specialized facilities [8]. Several alternative fabrication strategies have been implemented, including poly(dimethylsiloxane) (PDMS) devices [8,9]. There are several disadvantages involved in using PDMS devices; a major one being the solvent compatibil-

ity: PDMS is known to swell significantly in organic solvents, leading to leakage and device failure [10]. Although this article concentrates solely on aqueous systems, we will describe devices that are solvent resistant and therefore applicable to numerous applications in colloid and polymer science.

Our approach involves a rapid prototyping technique, originally developed for the fabrication of solvent resistant channels using a commercially available thiolene based optical adhesive. This technique is non-complex: it requires an uncollimated UV (365 nm) source, a mask, glass substrates and the thiolene resin. We refer the interested reader to the NIST publications [11–14] on device design and construction.

Under typical operating conditions, flow in microchannels is laminar: the spontaneous fluctuations on velocity that homogenize fluids in turbulent flows are dampened by viscous dissipation. Therefore, diffusion across these small channels is relatively slow. The distance along a channel for mixing to occur can be estimated from:

$$\Delta y_m \sim U(l^2/D), \quad (1)$$

where U is the average flow speed, l is the cross-sectional dimension of the channel, and D is the particle diffusivity [15]. The slower the flow speed, the better the mixing. However,

[☆] Contribution of the National Institute of Standards and Technology; not subject to copyright in the United States.

^{*} Corresponding authors.

E-mail address: anorman1@umd.edu (A.I. Norman).

¹ Current address: Department of Chemistry and Biochemistry, University of Maryland, College Park, MD 20742-2111, USA.

these devices are designed for *rapid* determination of morphology; particle size etc. so having a device containing a fluid flowing at a very slow rate is rather counterproductive. Stroock et al. [15] designed a mixing system in microchannels. This design allows for transverse components of flow that stretch and fold volumes over the cross section of the channel. Thus, the mixing length is reduced considerably. We show a design based on this device in order to reduce our mixing length.

This work focuses on the use of microfluidic devices to provide a screening tool for the study of a variety of aqueous based polymer formulations by small-angle light scattering (SALS). The model systems chosen for this study include polystyrene beads and poly(ethylene oxide) (PEO) diblock copolymers. These polymers form vesicles when dissolved in water. Vesicles are excellent candidates for controlled release vehicles. Applications of such materials include pharmaceuticals, agricultural and personal care products [16–18]. We have chosen a polymer which spontaneously forms vesicles on dissolution in water: EO₆BO₁₁, where EO is an ethylene oxide unit and BO is a butylene oxide unit. This polymer is known to form large (micron-sized) multilamellar vesicles and we refer the interested reader to a paper by Harris [19] on the formation and stability of these structures. The literature reports a number of EO based copolymers (mainly triblock Pluronics) where the vesicle structure has been investigated using Rheo-SALS [20–24]: The vesicle structure was induced by the application of shear, and the resulting vesicle structure (which is birefringent) characterized by a four-lobe pattern under depolarized SALS. To our knowledge, however, there have been no reports on SALS from polymer vesicles that are formed spontaneously when dissolved in water.

Microfluidic technology has been employed to elicit control over the self-assembly of liposomes. Jahn et al. [25] focused a lipid stream at a microfluidic T-junction between two buffer streams. The flow rates were adjusted to control the degree of hydrodynamic focusing and the width of the lipid stream, thus controlling the dilution process. Liposomes were formed, initially along the boundaries between the phospholipid and buffer. Such processes were characterized by fluorescence intensity measurements. It was shown that altering the flow rates in each channel could control liposome size. Demonstrations of the encapsulation process were also performed using fluorescent dyes.

This paper utilizes microfluidic techniques to mix polymer in an aqueous phase and probe the colloidal size using a custom small-angle light scattering (SALS) apparatus. We aim to show that this method can be used as a screening tool for the detection of specific particle sizes (the detectable range from approximately 800 nm to 25 μ m, given the wavelength of the incident radiation: 632.8 nm) and the formation of aggregated networks. We will demonstrate the ability of microfluidic devices to mix fluids using PS latex spheres, and then characterize the formation of vesicles using the block copolymer EO₆BO₁₁ in an aqueous stream.

We hope that this paper will demonstrate (using polymer vesicle formation as a specific example) how microfluidic technology, coupled with SALS, can eventually be used as a reliable

and rapid screening tool for the optimization of processing reaction conditions in materials science.

2. Materials and methods [26]

2.1. Materials

NOA 81 thiolene optical adhesive was purchased from Norland Products and used as received [27]. Acetone and ethanol (J.T. Baker and Warner-Graham, respectively) were used as received. A Jelight 342 UVO cleaner was used for ozonolysis of the glass substrates and a 365 nm Spectroline SB-100P floodlamp (equipped with a 100 W Hg lamp, Spectronics, NY) was used for the photo-polymerization of the NOA 81 resin. Polystyrene latex spheres (6 and 3 μ m) were purchased from Polysciences and used as received. The block copolymer EO₆BO₁₁ was obtained as a gift from the Dow Chemical Company and used as received.

2.2. Device fabrication

Negative photomasks were designed in Canvas software (version 7.0) and printed on overhead transparencies (3M, CG 3300) using a high-resolution laser jet printer (HP 8000N, 1200 dpi). Two masks were constructed (see Fig. 1a). One mask was the general device design, and the second mask, as shown in Fig. 1, revealed additional grooves within the device design to aid mixing. The two transparencies were weakly bound together on one edge using adhesive tape. NOA 81 optical adhesive was deposited onto a UVO cleaned glass slide (Corning 2947, 75 \times 1 mm). Four spacers (Silicon wafer pieces of 700 μ m) were placed in each corner of the coated glass slide to control the thickness. A second glass slide was lowered onto the liquid adhesive and gently placed on top of the first slide. A third glass, onto which the two transparencies are attached, was placed on to the two glass slides containing the optical adhesive. The device was photopolymerized so as to cross-link regions of the adhesive not shielded by the mask. This process involved three steps. (i) Precure of the adhesive: A UV intensity of 240 μ W/cm² was used and the device containing *both* transparencies was allowed to precure for 3 min 30 s. The upper transparency was then carefully removed, revealing the second transparency only (this was the mask containing the additional features within the mixing channels). This was then precured once more for 40 s. The curing time depends on the lamp intensity, the distance of the source to the device, and the desired feature heights [11]. Once precured, stainless steel needles (21 gauge) were inserted into the 3 entrance ports and the exit port of the device. The needles were fixed in position using thiolene resin (which was cured quickly by exposing these regions of the device to the UV lamp at distances of \sim 5 cm, which ensured rapid cross-linking). The uncured resin was then flushed from the channels with air, and a succession of ethanol and acetone. Ethanol and acetone solubilizes the uncured resin, however, acetone was used sparingly and immediately flushed out with ethanol, since it is known to swell the precured material and cause delamination of the device [14]. (ii) A sub-

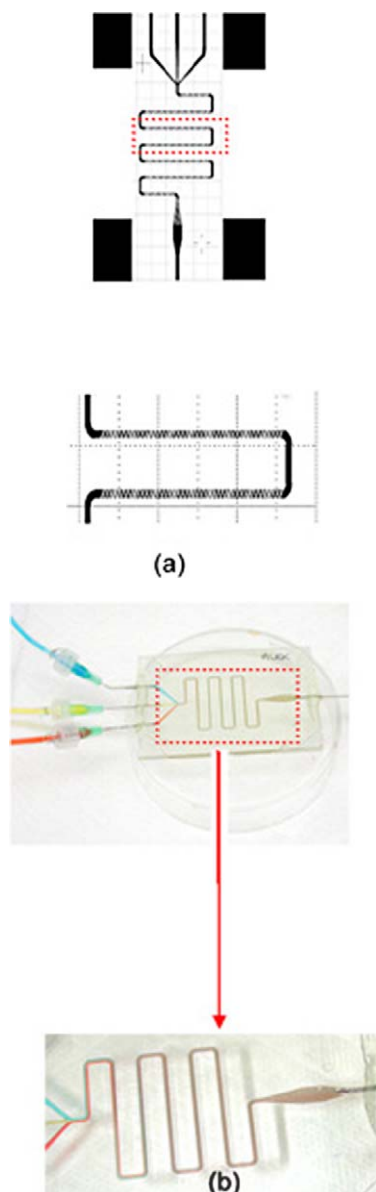


Fig. 1. (a) Negative photomask as designed using Canvas software (Ver. 7.0). Additional features within the device design are to aid mixing. Inlets are shown at the top of the mask for desired reactants, which flow through a mixing channel, and into the SALS viewing window, and finally reach the exit channel. (b) The mixing of colored components within a microfluidic device. Additional mixing features within the channels enhance the mixing process. Scale bar indicates 1 cm.

sequent post-cure was undertaken. This was performed at $\sim 5000 \mu\text{W}/\text{cm}^2$, which was achieved by placing the device directly under the lamp at a distance of ~ 10 cm for 15 min on each side of the device. (iii) Once post-cured, the device was then thermally cured at 50°C overnight. This post-curing process increases the solvent resistance, increases the adhesion to the glass substrate, and increases the mechanical stability via a higher cross-link density. All connections (entrance and exit ports) are sealed into position using epoxy resin (Elementis Specialties, Inc.). An example of the final device is shown in Fig. 1. The final dimensions in the device are: channel length, $L = 161$ mm, channel width, $W = 1.5$ mm and channel height

(given by the thickness of the silicon wafer spacers), $H = 0.7$ mm. The height of the grooves in the channel are dependent on the UV dosage and, in our case, are estimated to be $55 \mu\text{m}$.

2.3. Mixing studies

In order to simply visualize the extent of mixing in the microchannels, dilute solutions of household food dyes (red, blue and yellow) were prepared (a few drops of dye in ~ 10 mL of water) and drawn into syringes, which were screwed on to the entrance ports of the device. The syringes were then held clamped into Braintree (BS 8000) pumps to accurately control the flow rate. Flow rates of between 0.01 and 0.40 mL/min were employed in this study. Mixing occurs across small channel distances as indicated by visual evidence with the dyed solutions (Fig. 1b).

In order to quantify mixing of aqueous solutions of (1) $6 \mu\text{m}$ (standard deviation quoted as $0.354 \mu\text{m}$) and water and (2) 6 and $3 \mu\text{m}$ (standard deviation quoted as $0.145 \mu\text{m}$) Polybead polystyrene latex microspheres (Polysciences, Inc., PA) were mixed. $10 \mu\text{L}$ drops of PS microspheres were diluted in ~ 10 mL of deionized water. All solutions were refrigerated until used to prevent aggregation of the beads. The flow rates of each component that are required to achieve the defined concentrations are given in Table 1. The concentration of PS latex $6 \mu\text{m}$ spheres as purchased is 2.5 mg per 100 mL (2.5 wt%). Since $10 \mu\text{L}$ of PS latex sphere solution was dissolved in 10 mL of water, the concentration of PS spheres in the stock solution was 2.5×10^{-3} wt%. This was diluted further upon mixing within the channels. There were 2.10×10^5 particles/mL in the stock solution that we used. The estimated number of PS spheres that are scattered and detected is calculated by the scattering volume (1×1 (spot size) $\times 0.7$ mm (thickness of device)). This equates to 2.10×10^5 particles/mL $\times (0.7 \times 10^{-3}$ mL) = 147 PS latex spheres. The concentration and estimated number of PS latex spheres as a function of polymer flow rate are given in Table 1.

Solutions were loaded into 5 mL syringes and injected into the microfluidic device at the desired flow rate. The extent of mixing, in this case, was quantified by SALS. In all cases SALS patterns were acquired in the viewing region of the device a few minutes after cessation of flow. Initial SALS measurements were taken to assess the equilibration time for both the PS latex spheres and the block copolymer. In both cases 2 min proved to be sufficient.

To study the effect of salt on vesicle formation in the block copolymer, a 1.0 M stock solution of potassium bromide (KBr) was used and kept at a flow rate so as to keep the concentration at a constant 0.33 M. The flow rate was adjusted to vary the polymer concentration only.

2.4. Small angle light scattering (SALS)

SALS measurements were carried out using a custom light scattering apparatus, which is illustrated in Fig. 2. The apparatus consisting of a 15 mW HeNe laser (A) of wavelength 632.8 nm, and a set of optics to collimate the beam. An iris diaphragm (B) and a pinhole (C) vary the aperture range which

Table 1

Ratios of 6 μm PS bead solution in water (%) with respective flow rates (mL/min) used, the estimated number of PS latex spheres within the scattering volume and the PS bead concentration (wt%)

Ratio of flow rate of PS beads to the total flow rate (%)	Estimated number of PS latex spheres	$10^3 \times$ PS bead concentration (wt%)	Flow rate of PS bead solution (mL/min)	Flow rate of water (mL/min)
9.09	13.4	0.225	0.010	0.100
16.7	25.0	0.425	0.020	0.100
28.6	42.0	0.725	0.040	0.100
37.5	55.1	0.938	0.060	0.100
44.4	65.3	1.10	0.080	0.100
50.0	73.5	1.25	0.100	0.100
60.0	88.2	1.50	0.120	0.080
70.0	103	1.75	0.140	0.060
80.0	118	2.00	0.160	0.040
90.0	132	2.25	0.180	0.020
95.0	140	2.40	0.190	0.010
100	147	2.50	0.100	0

All quantities are given to 3 significant figures.

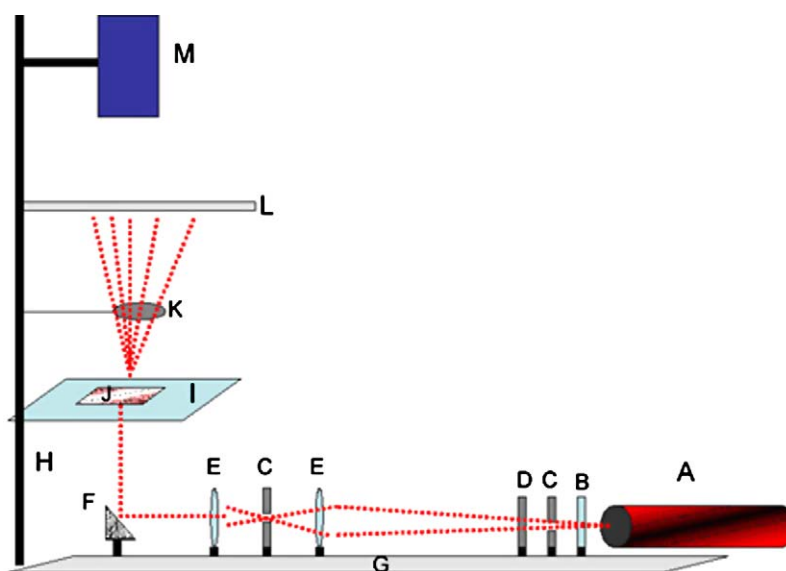


Fig. 2. A schematic illustration of the custom small-angle light scattering (SALS) apparatus. The laser beam is focused through an iris diaphragm, two planar convex lenses, a pinhole and after beam collimation hits a 45° mirror, where the laser beam is reflected 90° so as to hit the sample. The scattered light is collected on a diffuser plate and recorded using a CCD camera.

aids beam collimation. The beam is then shone through a polarizer (D) which acts as a neutral density filter and cuts out approximately 30% of the light, preventing any damage to the CCD camera. The beam is then reduced in size and focused through two planar convex lenses (E) with focal lengths $f_A = 25.4$ mm and $f_B = 62.9$ mm. The beam size is reduced to approximately 1 mm^2 . The collimated beam is then reflected 90° by a mirror (F) (held at 45°) so as to hit the viewing window of the microfluidic device (J), which is firmly clamped in position (H) on a motorized translation stage (I). Once the laser beam shines on the sample position, it is scattered over all directions. The scattered beam may be shone through an analyzer (K) (held on a retractable arm) which may be used for depolarized SALS. A beamstop constructed out of black Velcro (1 cm in diameter) is used to prevent the direct beam hitting the detector, a thermoelectrically cooled CCD camera (M) (14-bit, Apogee KX260E; the high bit depth of the CCD improved the signal to

noise ratio) collects the image of the scattering pattern which is projected on to a diffuser plate (L). The sample to diffuser plate distance was adjustable and is set to 0.25 m for our purposes.

A user-defined interface designed using LabVIEW software (version 8.0) controlled the sample position (via the translation stage), data acquisition and data reduction. All 2D images recorded by the CCD camera were reduced to a 1D $I(q)$ versus pixel number plot. This sector integration was performed in LabVIEW where the user sets specific parameters such as the position of the beam center and the radial resolution. The intensities on each pixel within the radial resolution set were added together to yield a 1D plot of scattered intensity, I , versus pixel number. The pixel number was then converted to scattering vector, q , where $q = (4\pi \sin \theta) / \lambda$ (θ is the scattering angle and λ is the wavelength). This was done by recording the scattering image of a diffraction grating of 1000 lines per inch, or 2500 lines per inch, dependent on the sample to diffuser distance, which

can be varied depending on the desired q range. The scattering vector, q is related to the microphase domain size, d , via $q = 2\pi n/d$, where n is the order of diffraction. The error in q is calculated from the uncertainty in the diffraction grating used, and is calculated as 0.4%.

All data was corrected for (i) bias frame (this is the offset that occurs when a pixel is read and accounted for by the subtraction of a zero length exposure with the shutter closed); (ii) dark current (this was produced by heat and was minimized by using a thermoelectric cooler. We account for this by a subtraction of a dark image from the data); (iii) flat field (this was due to each pixel having a slightly different sensitivity to light. We accounted for this by the division of a flat field frame from the data); and (iv) background scattering, which in our case is the solvent (water) held at rest in the microfluidic device. In all cases, the acquisition time was 3 s.

3. Results and discussion

3.1. Mixing studies 1: Colored dyes

Mixing was found to occur, at flow rates of 0.02 mL/min and below, in a microfluidic device (channel length, $L = 161$ mm, channel width, $W = 1.5$ mm and a channel height, $H = 0.7$ mm) that did not contain the additional grooves as described in our device fabrication section. Since high flow rates are advantageous in terms of the general high throughput approach, devices containing the grooves were tested and homogeneous mixing was observed at flow rates of up to 0.25 mL/min. At flow rates of greater than 0.25 mL/min, a gradient in color was observed at the viewing window. Fig. 1b displays the mixing of the three colored components at a flow rate of 0.20 mL/min. This figure is purely meant for illustrative purposes only and we do not attempt to quantify the mixing in any way using this approach.

3.2. Mixing studies 2: Polystyrene latex microspheres

In this section, we aim to demonstrate the ability of microfluidic SALS to measure sizes of colloids and to demonstrate mixing of two or more components. The SALS profiles of 6 μm

PS latex spheres and in water, at different flow rates (therefore at different concentration) are shown in Fig. 3. The ratio, shown in the legend in Fig. 3, is the wt% of PS latex spheres with respect to water.

At a PS latex sphere concentration of 2.25×10^{-4} wt% (corresponding to 13 PS spheres), characteristic oscillations in $I(q)$ are absent. This tells us about our instrument resolution: a concentration of greater than 2.25×10^{-4} wt% is required for the observation of oscillations in $I(q)$. Such oscillations arise from the scattering due to the *shape* of the particles. This term, the form factor, $P(q)$, is dependent on particle radius, R , and for particles with spherical symmetry, is given by Eq. (2) [28]:

$$P(q) = \left[\frac{3\{\sin(qR) - qR \cos(qR)\}}{(qR)^3} \right]^2. \quad (2)$$

A method of determining the particle size, d , is to determine the maximum (maximum peak height) of each peak position and calculate $d = 2n\pi/q$ (where n is the order of reflection). Table 2 summarizes this data. The first three orders of reflection result in an error lying within one standard deviation of the sizes quoted by Polysciences, Inc. (99% confidence). The fourth and

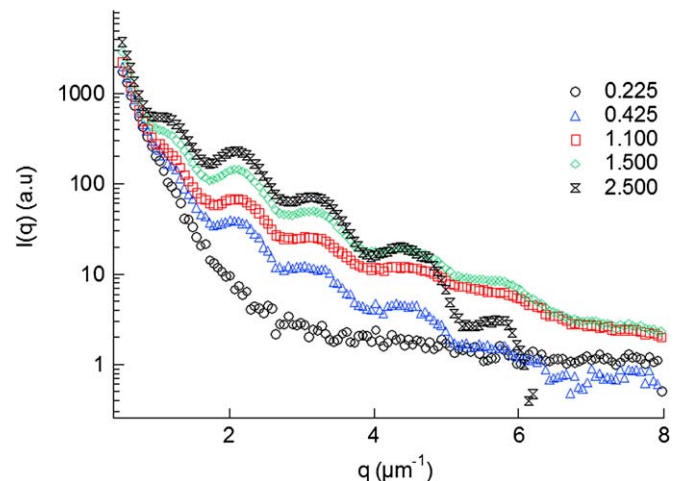


Fig. 3. SALS profiles of a solution of 6 μm PS beads and pure water. Legend indicates the concentration ($\times 10^{-3}$ wt%) of PS bead solution in water as determined by the flow rate.

Table 2
Domain spacing, or particle diameter, as probed by SALS from each order of reflection in $I(q)$

Ratio of PS beads to water (%)	Estimated No. of PS beads	$10^3 \times$ PS bead conc. (wt%)	1st order (μm)	2nd order (μm)	3rd order (μm)	4th order (μm)	5th order (μm)
9.09	13.4	0.225	N/A	N/A	N/A	N/A	N/A
16.7	25.0	0.425	5.72	5.90	5.85	5.48	5.42
28.6	42.0	0.727	5.72	5.74	5.85	5.48	5.32
37.5	55.1	0.938	5.72	5.90	5.75	5.48	5.37
44.4	65.3	1.10	5.72	5.74	5.75	5.48	5.47
50.0	73.5	1.25	5.72	5.74	5.85	5.48	5.42
60.0	88.2	1.50	5.72	5.74	5.75	5.55	5.42
70.0	103	1.75	5.72	5.74	5.75	5.54	5.42
80.0	118	2.00	5.72	5.74	5.75	5.55	5.47
90.0	132	2.25	5.72	5.74	5.75	5.54	5.42
95.0	140	2.40	5.72	5.74	5.75	5.54	5.42
100	147	2.50	5.72	5.74	5.75	5.54	5.47

All quantities are given to 3 significant figures.

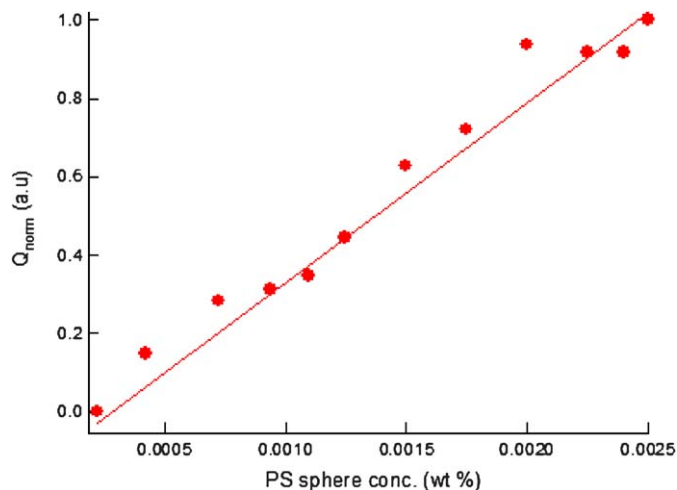


Fig. 4. The normalized total scattered intensity, Q , as a function of polystyrene latex sphere concentration.

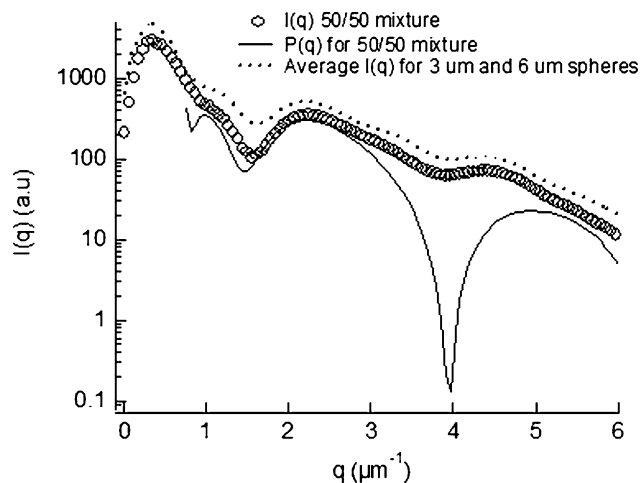


Fig. 5. SALS profile from a solution of a 1:1 mixture of 3 and 6 μm PS latex spheres (open circles), with the corresponding theoretical (solid line) and experimental (broken line) predictions.

fifth orders calculate a size regime within a 95% confidence limit.

The total scattered light over the given q range has been calculated (by the summation of intensities at each q value) and plotted as a function of PS latex sphere concentration in Fig. 4. The relation between these two variables is approximately linear, which leads us to conclude that mixing in the microfluidic channels is uniform for this system.

The extent of mixing can also be shown by incorporating different sized PS latex spheres in the microfluidic device. A precise method of determining how well such components mix is to compare experimental data to theoretical data. The theoretical prediction, for a 1:1 mixture (in terms of wt%) of each component is taken as the mean average of the form factors, $P(q)$, calculated from Eq. (2), for each component. This is shown in Fig. 5. As shown, the positions of the peaks match well with the experimental data. In addition, a prediction of $I(q)$ based on existing data is calculated. This was calculated by the addition (in equal quantities) of the SALS profiles for 3 μm PS spheres

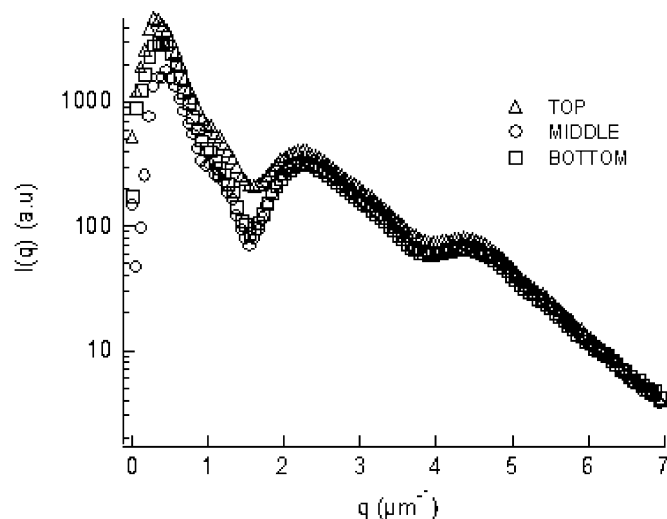


Fig. 6. SALS profile from a 1:1 mixture of 3 and 6 μm PS spheres, at the top (triangles), middle (circles) and bottom (squares) of the viewing window of the microfluidic device.

and 6 μm PS spheres, and then dividing the result by a factor of 2. The predicted scattering profile has the same shape as the observed data, although there are slight variations in intensity. Such observations are consistent with homogeneous mixing throughout the microfluidic device. To confirm that mixing was in fact homogeneous, SALS data has been recorded with the laser focused onto different regions of the SALS viewing window of the device: (i) at the top of the window close to the walls of the channel, (ii) in the middle of the window (where the majority of experiments have been performed), and (iii) at the bottom of the window close to the walls of the channel. The chip is moved transverse to the flow direction to accommodate this. As Fig. 6 shows, mixing is shown to be consistent in terms of having almost identical scattering patterns over all regions of the window for a 1:1 mixture of 3 and 6 μm PS spheres.

3.3. Mixing studies 3: Vesicles formed from $\text{EO}_6\text{BO}_{11}$ in water

The mixing of $\text{EO}_6\text{BO}_{11}$ and water was achieved by setting the maximum flow rate so as to not surpass 0.20 mL/min, thus allowing for homogeneous mixing of each component. The SALS data is shown in Fig. 7. The inset to Fig. 7 shows the 2D data. Unlike the PS latex spheres, the vesicles show a broad size distribution, resulting in the peaks smearing over the beamstop region. The main feature of such data is the overall increase in scattered intensity as the concentration of polymer increases. The peak position also appears to move to a slightly higher q value. This would suggest a reduction in the vesicle size. However, since this peak is so broad, it makes the quantitative analysis of vesicle size rather difficult.

Since the correlation peak is smeared over the beamstop region, it is impossible to obtain a specific size for the vesicles in question. It is only concluded, from SALS data alone, that there is a broad range of particle size as the two liquids mix. In order to quantify the size regime, an indirect Fourier transform is performed on the data to extract the pair distance distribution function, $p(r)$, which is related to the scattered intensity by the

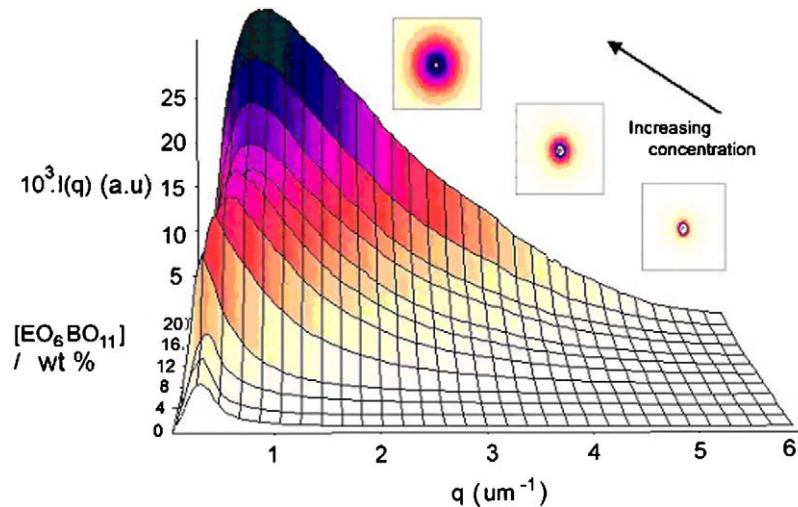


Fig. 7. Circularly averaged SALS data: $I(q)$ vs q as a function of polymer concentration (which is proportional to the relative flow rate). The inset shows the original 2D SALS data.

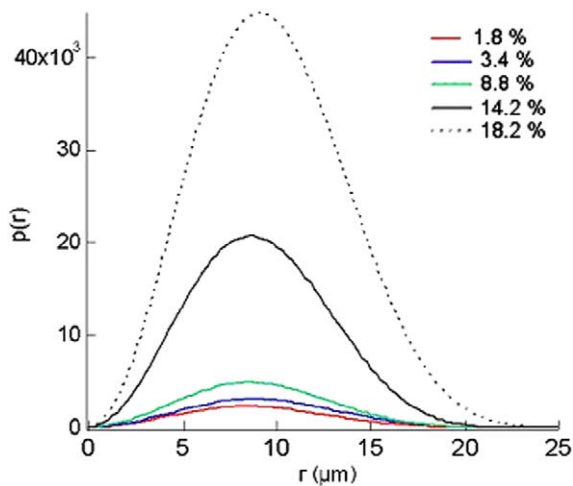


Fig. 8. Pair distance distribution function, $p(r)$, vs r for a range of concentration of $\text{EO}_6\text{BO}_{11}$ diblock copolymer in aqueous solution (wt%).

following:

$$I(q) = 4\pi \int_0^{\infty} p(r) \frac{\sin(qr)}{qr} dr. \quad (3)$$

The $p(r)$ function has been described in great depth by Glatter et al. [28] and the interested reader is referred to references therein.

The $p(r)$ functions are calculated and shown in Fig. 8. The symmetric curve is a result of the spherical nature of the scattering object. Should an elongated structure be present, such as a rod-like or a disk-like object, this would be reflected by an asymmetric curve. The $p(r)$ function increases in intensity as the concentration increases. This is due to an increase in concentration of scattering objects (vesicles). Using the analogy that the $p(r)$ function can be crudely thought of as a probability distribution function of scattering objects of varying size; it is concluded that there is a broad distribution of vesicle size within the samples in question. This results in SALS profiles

without a distinct peak. The $p(r)$ peak position, indicative of the most probable particle dimension appears to remain approximately the same, 9 μm . The maximum particle dimension is defined as the point to which $p(r)$ falls back to zero and is within the range 20–25 μm . From these data, and the fact that there are always errors in obtaining a q range, all dimensions from the $p(r)$ can be regarded as the same *within experimental uncertainties*. We conclude that the vesicle size of $\text{EO}_6\text{BO}_{11}$ in water does not change as a function of polymer concentration. The inverse Fourier transformation of SALS data does suggest, to some degree, that as the concentration of polymer increases, the size distribution of vesicles is increased. This can be explained purely by the fact that as the concentration of vesicles increases, the population of large micron-sized vesicles increases and become detectable by SALS. Overall, as the concentration increases there is no notable change in the size or the size distribution of the vesicles.

The devices described throughout this paper have also been used to incorporate salt solution in addition to vesicle forming polymers. Examples of acquired data are shown in Figs. 9a and 9b. Fig. 9a shows an increase in intensity and a shoulder becoming evident off the beamstop region. Such observations are consistent with the formation, and interaction of vesicles. Fig. 9b compares data with and without the addition of salt. It is clear that on addition of salt, vesicles form at a lower concentration and the effect is highly pronounced: a five fold increase in intensity is observed at $\sim q = 2 \mu\text{m}^{-1}$ for the polymer/salt solution. Increasing the concentration of salt was found, as expected, to reduce the concentration at which vesicles were observed. We postulate that this is brought about by the competition that exists between the polymer and the K^+ and Br^- ions for the “free” water available. The ions become hydrated and thus reduce the concentration of “free” water, thus increasing the effective concentration of polymer. Hence, vesicles are observed at a lower polymer concentration, and the observed scattered intensity is increased. The two peaks observed at ca. 4.5 and 5.0 μm^{-1} are due to edge effects of the detector. The increase in number of vesicles causes an increased illumination

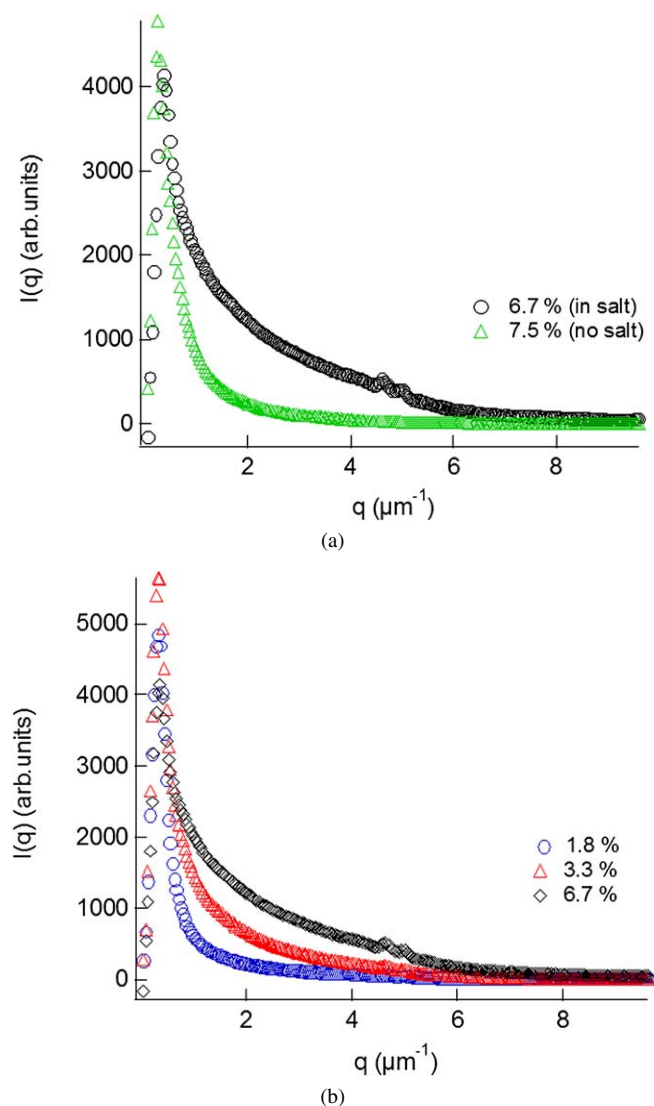


Fig. 9. (a) Circularly averaged SALS data: $I(q)$ vs q as a function of polymer concentration (wt%) for one system with the addition of KBr (aq) and one without. (b) Time-resolved circularly averaged SALS data: $I(q)$ vs q as a function of polymer concentration in 0.33 M KBr (aq) solution.

of the scattered beam. This increased illumination magnifies the scattering due to the edges of the diffuser plate.

The vesicle size observed by SALS and subsequent inverse Fourier transformation (IFT) is approximately three orders of magnitude greater than the vesicle membrane thickness (which has been observed using SANS techniques [29]): on the order of microns compared to nanometers. SANS studies suggested the existence of *smaller* unilamellar vesicles. However, such large structures as those determined in this study would be too large to be studied by SANS. Similarly, the unilamellar vesicles as detected by SANS are too small for detection by SALS. We therefore propose that the polymer EO₆BO₁₁ (when dissolved in water) exists as a mixture of unilamellar vesicles and multilamellar vesicles. These dimensions provide a sufficiently large hollow region to encapsulate materials, such as drugs, or to perform chemistry within such structures. The behavior of such structures in a buffer solution (such as saline solution) is

an integral part of drug delivery design and performance. Understanding the way in which such systems behave at elevated temperatures (e.g., at body temperature), also, is a key issue for this application. In the future we hope to incorporate a heating element to *rapidly* investigate vesicle structure as a function of temperature (and other external influences such as pH) on vesicle formation.

4. Conclusions

A microfluidic device designed for mixing two or three fluid components proved reproducible, robust and versatile. Introduction of grooves within the channels aided mixing substantially and allowed mixing of components at enhanced flow rates, thus reducing the time necessary for each experiment.

The mixing of PS latex microspheres provided a demonstration of uniform mixing within the microchannels, relating the flow rate of each component to the SALS intensity observed to yield the respective composition. In addition, such samples were used to characterize the mixing process as a function of position on the viewing window of the device. Mixing was shown to be homogeneous across the channel width.

The capabilities of our device were demonstrated with measurements on a vesicle-forming polymer as it mixes with water, both with and without the addition of a salt solution. The SALS data shows the formation of vesicles over a period of a few minutes. Hence a 2-min equilibration time after each flow rate change was necessary before recording the SALS spectra. A gradual increase in $I(q)$ was observed with increasing polymer concentration, but this was substantially increased when the polymer concentration reached 5.8 wt%. Such an increase continued until the limit of 20 wt% polymer. The scattered intensity observed was very broad and was smeared over the beamstop; no distinct peak was resolved, indicating the formation of very large, polydisperse vesicle structures. An inverse Fourier transform was applied to all data, yielding the pair distance distribution function, $p(r)$. This function estimated a mean size of $\sim 9 \mu\text{m}$, which is an observed three orders of magnitude higher than their respective membrane thicknesses. We also conclude, using information gathered from SANS studies [29] that the polymer EO₆BO₁₁ can exhibit both unilamellar and giant multilamellar vesicles when dissolved in water at low concentrations. The addition of a third component, a 0.1 M KBr (aq) solution, resulted in the formation of vesicles at a lower observed polymer composition.

The experiments described in this work demonstrate a rapid, economic screening method for polymer solutions. For example, using SALS coupled with such devices, it is possible to assess a multitude of solution conditions quickly and effectively (using a minimum amount of reactants and solvents). Optimum conditions can be discovered this way. Such screening techniques may be used for many applications. Examples include pH-responsive vesicles [30] that form one structure in acidic conditions and the reverse structure under basic conditions. At intermediate pH these materials form spherical and ellipsoidal aggregates. The vesicle structure, of ionic surfactants, can also be broken down by the addition of multivalent ions and

monitored in such a device. Complimentary techniques, such as Fluorescence spectroscopy, can be used to monitor the release of material under a variety of conditions. SALS can be used, as described, to monitor the vesicle structure as a function of (a) polymer concentration, (b) solvent ratio, and (c) ionic strength. Such applications will depend highly on the membrane rigidity of such materials, which may also be probed using scattering methods (light, X-ray and neutron) coupled with such microfluidic technology.

Acknowledgments

We acknowledge Dr. Zuzanna Cygan (NIST) for valuable discussions on device design, and assistance with device fabrication. We also thank Drs. Alamgir Karim and Michael Fasolka for useful discussions and continued support throughout this project. This work was carried out at the NIST Combinatorial Methods Center (NCCM). More information is available at <http://www.nist.gov/combi>.

References

- [1] C. Hansen, S.R. Quake, *Curr. Opin. Struct. Biol.* 13 (2003) 538.
- [2] T.S. Sammarco, M.A. Burns, *AIChE J.* 45 (1999) 350.
- [3] H.-P. Chou, C. Spence, A. Scherer, S.R. Quake, *Proc. Natl. Acad. Sci. USA* 96 (1999) 11.
- [4] D.A. Dunn, L. Feygin, *Drug Discov. Today* 5 (2000) S84.
- [5] M.W. Losey, M.A. Schmidt, K.F. Jensen, *Ind. Eng. Chem. Res.* 40 (2001) 2555.
- [6] J. Ouellette, *Ind. Physicist* 14 (August/September 2003).
- [7] A. Scherer, S.R. Quake, *Science* 290 (2000) 1536.
- [8] J.C. McDonald, G.M. Whitesides, *Acc. Chem. Res.* 35 (2002) 491.
- [9] J.M.K. Ng, I. Gitlin, A.D. Stroock, G.M. Whitesides, *Electrophoresis* 23 (2002) 3461.
- [10] J.N. Lee, C. Park, G.M. Whitesides, *Anal. Chem.* 75 (2003) 6544.
- [11] C. Harrison, J.T. Cabral, C.M. Stafford, A. Karim, E.J. Amis, *J. Microchem. Microeng.* 14 (2004) 153.
- [12] J.T. Cabral, S.D. Hudson, C. Harrison, J.F. Douglas, *Langmuir* 20 (2004) 10020.
- [13] T. Wu, Y. Mei, J.T. Cabral, C. Xu, K.L. Beers, *J. Am. Chem. Soc.* 126 (2004) 9880.
- [14] Z.T. Cygan, J.T. Cabral, K.L. Beers, E.J. Amis, *Langmuir* 21 (2005) 3629.
- [15] A.D. Stroock, S.K.W. Dertinger, A. Ajdari, I. Mezić, H.A. Stone, G.M. Whitesides, *Science* 295 (2002) 647.
- [16] D.D. Lasic, in: M. Rossoff (Ed.), *Vesicles*, Dekker, New York, 1996, p. 448.
- [17] C. Allen, D. Maysinger, A. Eisenberg, *Colloids Surf. B* 16 (1999) 3.
- [18] J. Ding, G. Liu, *J. Phys. Chem. B* 102 (1998) 6107.
- [19] J.K. Harris, G.D. Rose, M.L. Bruening, *Langmuir* 18 (2002) 5337.
- [20] J. Zipfel, J. Berghausen, G. Schmidt, P. Lindner, P. Alexandridis, M. Tsianou, W. Richtering, *Phys. Chem. Chem. Phys.* 1 (1999) 3905.
- [21] O. Diat, F. Nallet, D. Roux, *J. Phys. II* 3 (1993) 1427.
- [22] J. Bergholtz, N. Wagner, *Langmuir* 12 (1996) 3122.
- [23] J. Zipfel, P. Lindner, M. Tsianou, P. Alexandridis, W. Richtering, *Langmuir* 15 (1999) 2599.
- [24] F. Nettesheim, U. Olsson, P. Lindner, W. Richtering, *J. Phys. Chem. B* 108 (2004) 6328.
- [25] A. Jahn, W.N. Vreeland, M. Gaitan, L.E. Locascio, *J. Am. Chem. Soc.* 126 (2004) 2674.
- [26] Certain commercial equipment, instruments or materials are identified in this paper to specify the experimental procedure. Such identification is not intended to imply recommendation by the National Institute of Standards and Technology, nor is it intended to imply that the materials or equipment identified are necessarily the best available for the purpose.
- [27] Technical data sheet for NOA Optical Adhesives, Norland Products, Inc., New Brunswick, NJ.
- [28] O. Glatter, in: P. Lindner, T. Zemb (Eds.), *Neutrons, X-Rays, and Light: Scattering Methods Applied to Soft Condensed Matter*, Elsevier, Amsterdam, 2000.
- [29] A.I. Norman, D.L. Ho, J. Lee, A. Karim, *J. Phys. Chem. B* 110 (2006) 62.
- [30] F. Liu, A. Eisenberg, *J. Am. Chem. Soc.* 125 (2003) 15059.